Available online at www.sciencedirect.com

jmr&t Journal of Materials Research and Technology

www.jmrt.com.br

Original Article

Effects of rust layer and corrosion degree on the pullout behavior of steel fibers from ultra-high-performance concrete

Doo-Yeol Yoo, Jae Young Gim, Booki Chun *

Department of Architectural Engineering, Hanyang University, 222 Wangsimni-ro, Seongdong-gu, Seoul, 04763, Republic of Korea

ARTICLE INFO

Article history:
Received 27 December 2019
Accepted 29 January 2020
Available online 8 February 2020

Keywords:
Ultra-high-performance concrete
Surface corrosion
Straight steel fiber
Pullout resistance
Rust layer
Surface roughness

ABSTRACT

This study investigates the effect of surface corrosion on the pullout behavior of straight steel fibers embedded in ultra-high-performance concrete (UHPC). To this aim, straight steel fibers, either with or without surface corrosion, were utilized, and various corrosion degrees from 2% to 15% by weight were considered. To evaluate the implication of rust layer on the pullout behavior of corroded steel fibers from UHPC, both washed and unwashed conditions were considered. The surface roughness of plain and corroded steel fibers was analyzed by means of scanning electron microscope and atomic force microscope (AFM) images. The test results indicated that surface corrosion is effective in enhancing the pullout resistance of straight steel fibers in UHPC when the fibers are completely pulled out from the matrix without breakage. The maximum average bond strength and pullout energy of moderately corroded fibers in UHPC were found to be 18.5 MPa and 715.7 N·mm, approximately 2.7 and 1.8 times higher than those of plain fibers in the same matrix at the aligned condition. The benefits of moderate surface corrosion on improving the pullout resistance were mitigated by inclining the fibers. A higher corrosion degree led to a better pullout resistance up to a certain value (2 or 5%); however, beyond such value, the resistance decreased significantly due to the rupture of fibers. A threshold value of 2% for the corrosion degree was thus suggested to achieve an excellent fiber bridging capability. The washed corroded fibers exhibited higher bond strength and pullout energy than the unwashed ones with the same degree of corrosion at aligned condition; however, the benefits of washing vanished when the fibers were inclined and ruptured prematurely. An obvious correlation between the bond strength and the surface roughness was observed from the AFM images.

1. Introduction

To overcome some drawbacks of ordinary concrete (e.g., high brittleness, relatively low tensile-to-compressive strength ratio, and insufficient flowability), a reactive powder concrete (RPC), which is a precursor of ultra-high-performance concrete (UHPC) now commercially available worldwide, was first introduced by French engineers in the mid-1990s [1]. Because of its high compactness, which results from the optimization of particle packing and the high volume of micro straight steel fibers, it generally exhibits excellent mechanical properties (a compressive strength greater than 150 MPa and a designed

* *Corresponding author.*
E-mail: boogi0354@hanyang.ac.kr (B. Chun).

https://doi.org/10.1016/j.jmrt.2020.01.101

tensile strength of 8 MPa [2,3]), resistance to fatigue, and durability. In particular, Voort [4] summarized the properties of durability of UHPC compared to those of high-performance concrete (HPC) and normal concrete (NC). According to his reports, UHPC has a significantly higher resistance to chloride ion and gas permeability compared to that of HPC and NC. For instance, the resistance to chloride ion and oxygen permeability of UHPC are 34 and 10 times greater than that of HPC, respectively, and 220 and 100 times greater than that of NC, respectively. The excellent permeability resistance of UHPC is due to densely packed microstructures, which form thanks to a very low water-to-binder (W/B) ratio and inclusions of high-fineness admixtures and a defoaming agent. For this reason, Shaheen and Shrive [5] reported that the corrosion of steel fibers included in UHPC can be very slow, although the steel fibers exposed at a crack may be corroded.

A number of previous studies [6–12] have evaluated the corrosion of reinforcing bars made of conventional steel embedded in fiber-reinforced concrete (FRC), and observed the effectiveness of the added fibers in improving the resistance to corrosion of the steel bars. Hou and Chung [7] examined the effect of admixtures on the corrosion resistance of steel bars embedded in concrete, and reported that the addition of silica fume and latex effectively improves the corrosion resistance, whereas carbon fibers have a negative effect on such resistance because of the reduced electrical resistivity. Based on the steel bar corrosion test results using plain mortar and FRCs with steel cord and polyethylene (PE) fibers, Mihashi et al. [8] recommended using hybrid steel cord and PE fibers for enhancing the corrosion resistance of reinforcing steel bars, demonstrating its superior performance compared to single PE fibers and plain mortar. Similarly, Blunt et al. [6] and Jen and Ostertag [9] estimated the efficiency of using hybrid polyvinyl alcohol (PVA) fiber and hooked-end steel fiber on the corrosion resistance of reinforced concrete. They [6] initially conducted cyclic flexural loading tests of reinforced concrete and hybrid FRC, and evaluated their corrosion rates. The hybrid FRC delayed the initiation of corrosion, and reduced the active corrosion rate compared to that in plain concrete because of the propensity of high crack resistance. Jen and Ostertag [9] also reported that the most impactful consequence of fiber reinforcement is the suppression of corrosion-induced splitting cracks in concrete structures. This can effectively extend the lifespan of these structure prior to overcoming the threshold of acceptable damage, which is given by the *fib* Model code [13]. Berrocal et al. [10] compared the corrosion resistance of steel rebars in uncracked and cracked plain concrete and FRCs with steel and PVA fibers, and concluded that PVA fibers or hybrid steel and PVA fibers are efficient in delaying the initiation of corrosion, whereas the steel fiber alone does not provide any advantage compared to the use of plain concrete.

Due to the incorporation of micro steel fibers, the RPC belongs to the category of steel-fiber-reinforced concrete (SFRC). It has been used frequently for several structural elements (e.g., slab-on-grade, pedestrian bridge decks, tunnel linings [14–17]). Although the commercial steel fibers used for RPC (or UHPC) are brass-coated and it is known that the corrosion of SFRC is slower than that of steel rebars, there exists the possibility of surface corrosion. However, fewer studies [18–24] are available regarding the corrosion of steel fibers in concrete compared to those focusing on steel rebar corrosion. In the late 1980s, Banthia and Foy [21] examined the pullout behavior of hooked-end steel fibers in cement matrix after exposure to marine environment for up to one year, and reported several important findings: (1) marine curing at low temperature (2 °C) did not adversely affect the pullout resistance of the steel fiber even after one year of exposure: (2) high temperatures (22 and 38 °C) promoted the early corrosion of the steel fiber in marine environment, causing an increase of bond strength due to the lateral confinement of the fiber caused by oxidation in some cases (e.g., early ages); and (3) the deformed portion (end-hook) of the steel fiber is susceptible to anodic oxidation by the extant residual stress. Kosa and Naaman [19] conducted an experimental investigation of the effects of steel fiber corrosion, resulting from immersion in a 3.5% standard sodium chloride (NaCl) solution, on the mechanical properties (including the strength and toughness) of the FRC. The authors reported that both the strength and toughness of the FRC decreased after a certain degree of corrosion owing to the reduced minimum fiber diameter. It was also found that the decrease of toughness was much more pronounced compared to that of the strength [19]. Frazão et al. [18] reported that the main corrosion products, formed uniformly on the entire fiber surface under the 3.5% NaCl solution, are iron oxides, and the pullout strength of the hooked steel fiber in self-consolidating concrete increases with the crack width ranging from 0.1 mm to 0.5 mm after 10 days of immersion in the solution because the corrosion products increases the surface roughness. Similarly, Granju and Balouch [20] experimentally verified the increase in the flexural strength due to steel fiber corrosion of pre-cracked SFRC beams exposed to a marine-like environment for one year. Hashimoto et al. [22] evaluated the diffusivity of chloride ions and the tensile behavior of an ultra-high-strength concrete (UHSC) having a similar mix proportion and curing process to those of the UHPC, reinforced with steel fibers under corrosive environment (i.e., exposed to seawater) to investigate the effect of initial crack width. Insignificant steel fiber corrosion and chloride ion penetration was found in the non-cracked UHSC samples after up to 6 months, whereas the chloride ion was deeply and widely dispersed, and the steel fibers were obviously corroded, in samples with initial crack width of 0.5 mm or wider, which is consistent with the findings of Granju and Balouch [20]. The initiation of corrosion of the steel fibers increased the tensile stress carrying capacity of the UHSC regardless of the initial crack width [22].

Similar to the studies discussed above, most of the previous studies on steel fiber corrosion have been carried out using ordinary SFRC, and very limited studies [22,25,26] are available on the corrosion of steel fibers in UHPC and its effects on the mechanical properties. Hashimoto et al. [22], Pyo et al. [25], and Abbas et al. [26] noted consistently that UHPC can effectively resist the penetration of chloride ion due to its dense microstructure; on the other hand, UHPC with cracks suffers from steel fiber corrosion, which affects its tension-softening characteristics [22]. It has been reported that UHPC is highly susceptible to shrinkage cracks during the manufacturing stage because of its steep increase of early-age autogenous shrinkage, a thin cross-sectional dimension,

Table 1 – Chemical compositions and densities of cement and silica fume.

Composition %	Cement*	Silica fume
CaO	61.33	0.38
Al_2O_3	6.40	0.25
SiO_2	21.01	96.00
Fe_2O_3	3.12	0.12
MgO	3.02	0.10
SO_3	2.30	–
Density (g/cm^3)	3.15	2.10

* Type I Portland cement.

Table 2 – Details of mixture proportion of UHPC.

W/B[b]	Mix design [kg/m^3]					
	Water	Cement	Silica fume	Silica sand	Silica flour	SP[a]
0.2	160.3	788.5	197.1	867.4	236.6	52.6

[Note] W/B = water-to-binder ratio and SP = superplasticizer.

[a] Superplasticizer includes 30% solid (= 15.8 kg/m^3) and 70% water (=36.8 kg/m^3).

[b] W/B is calculated by dividing total water content by total amount of binder.

etc. [27,28]. The post-cracking tensile behavior of UHPC is also significantly affected by the properties of the interfacial bond between the fiber and the matrix; thus the pullout response of corrosion-induced steel fibers from the UHPC matrix must be examined to fundamentally understand its tensile behavior. Unfortunately, to the authors' best knowledge, no published studies are available on this matter, and to address this lack of understanding, this study first investigated the impact of the degree of corrosion of steel fibers in UHPC on its pull-out behavior. For an innovative data analysis, the impact of corrosion degree on the surface conditions, considering the surface roughness and rust layer, of steel fibers was quantitatively evaluated through energy-dispersive X-ray spectroscopy (EDX) mapping on scanning electron microscope (SEM) image and atomic force microscope (AFM) image analysis. It was verified that the interfacial bond properties of steel fibers in UHPC are strongly affected by corrosion, in a way that depends on the degree of surface corrosion.

2. Materials and methods

2.1. Ingredients and mix proportion for the UHPC

For fabricating UHPC, type I Portland cement and Elkem Microsilica – Grade 940U silica fume (SF) were used as cementitious materials. Their chemical compositions and densities are given in Table 1. For obtaining mean particle sizes of dry ingredients, a particle size distribution analysis was conducted three times for each ingredients (from an identical package), excluding the SF. For the case of SF, the analysis was performed twice from separately ordered packages. The mean particle sizes of cement and SF were then found to be 22 μm (S.D. of 0.49 μm) and 0.31 μm (S.D. of 0.11 μm), respectively [29], where S.D. indicates the standard deviation. As fine aggregate and filler for achieving high packing density, silica sand and silica flour were utilized. Their mean particle sizes were found to be 337 μm (S.D. of 5.24 μm) and 4.2 μm (S.D. of 0.04 μm), respectively; the latter was primarily composed (> 98%) of silicon dioxide (SiO_2). Although the incorporation of coarse aggregate in the UHPC mixture has several advantages (high flowability, less mixing time, less amount of cementitious materials, etc.) without sacrificing the compressive strength, no coarse aggregates were included in the mixture, to maintain a similar composition to that of ordinary UHPC available in North America [30], due to the deterioration of fiber pull-out resistance. In accordance with several international codes for UHPC [2,3], its minimum compressive strength needs to be greater than 150 MPa. The water-to-binder (W/B) ratio is one of the factors influencing the strength of concrete the most: a lower W/B ratio leads to a higher strength. Thus, a very low W/B ratio (0.2) was adopted. To achieve self-consolidating characteristic, a high-range water-reducing admixture, i.e. a polycarboxylate superplasticizer (SP) with 30% solid and 70% water, was incorporated. The detailed mixture proportion is summarized in Table 2.

By using a Hobart-type mixer, all the dry ingredients (i.e., cement, SF, silica flour, and silica sand) were pre-mixed for 10 min at a mixing speed of 90 rpm (revolutions per minute); subsequently, water mixed with SP was incorporated and mixed further for 5 min. Once the mixture became flowable, a flow table test was conducted according to ASTM C1437 [31], and the average flow value of approximately 230 mm was obtained.

2.2. Process of steel fiber corrosion

According to an earlier study conducted by Frazão et al. [18], a standard 3.5% NaCl solution can be used for obtaining corroded steel fibers. To examine the effect of the degree of corrosion on the pullout response of straight steel fibers from the UHPC matrix, various degrees of fiber corrosion were obtained, ranging from 0% to 15%, which were assessed by the weight ratio. Because the weight of the single steel fiber is small, a bundle of ten fibers was used for monitoring the corrosion degree three times a day by using a high-accuracy balance with a precision of 0.001 g. For this, commercial smooth, straight steel fiber with a diameter of 0.3 mm and a length of 30 mm was adopted. Its ultimate tensile strength, elastic modulus, and density were 2,500 MPa, 200 GPa, and 7.9 g/cm^3, respectively. When the steel fibers were kept immersed in the NaCl solution, the process of fiber corrosion was fairly slow. Therefore, to accelerate the corrosion process, the steel fibers were immersed in the NaCl solution for 18 h, and then they were left to dry by exposing them to the atmosphere. This process was repeated until the desired corrosion degrees were obtained (i.e., 2, 5, 10, and 15%). The corrosion degree was evaluated after eliminating a rust layer which had formed on the surface of the fiber using absolute alcohol. The corroded fibers were immersed into absolute alcohol for 5 min, and then they were cleaned with a wiper applied along the longitudinal direction of the fiber. Such a cleaning process was continued until no impurity substance was detected from the wiper after rubbing slightly.

To estimate the effect of the rust layer on the pullout resistance of steel fibers in UHPC, washed and unwashed, corroded fibers were prepared. The unwashed, corroded fibers were immediately stored in an airtight container once the desired corrosion degree was achieved. On the other hand, an additional cleaning process was applied to obtain the washed, corroded fibers. The cleaning process for the latter was as follows: the corroded fibers were immersed in absolute alcohol for 5 min and cleaned using a brush; then, the fibers were immersed into absolute alcohol again, and stirred using a Hobart-type mixer for 30 s (speed of 90 rpm); finally, the fibers were extracted from the mixer, dried in a laboratory room for 2 h with a temperature of about 20 °C, and stored in the airtight container. The AFM images were taken by a XE-100 AFM machine, and cover an area of $40 \times 40\ \mu m^2$. To increase the accuracy of image analysis, the size of 3D images decreased to an area of $35 \times 35\ \mu m^2$, based on an elimination of the eccentricity of edges.

The test materials in this study can be subdivided into three types: 1) plain fibers, 2) unwashed, corroded fibers, and 3) washed, corroded fibers. The initial letter C denotes the corroded fibers, and the sequential numeral indicates the corrosion degree. The last letters U and W indicate the unwashed and washed, corroded fibers, respectively. For example, the code C02U refers to unwashed, corroded fibers with a corrosion degree of 2%.

2.3. SEM-EDX measurements

To visually grasp the changes of appearance and roughness on the fiber surface according to the degree of corrosion, SEM-EDX analysis was conducted. Both the plain and corrosion-induced steel fibers with a diameter of 0.3 mm and a length of 30 mm were inserted into the high resolution SEM machine. The EDX is a device that is attached to the detector of SEM and capable of qualitatively and quantitatively analyzing chemical components in microstructure from the characteristic X-rays among various signals emitted by the interaction between the sample surface and electron beam. Three major elements, such as iron (internal component of fiber), copper (main component of brass-coating for corrosion protection), and oxygen which can be produced by oxidation of iron, were filtered for evaluating the corrosion degree of fiber surface. The distribution of the chemical elements was mapped to estimate the extent of oxidation, due to corrosion in an entire measurement area.

2.4. Specimen preparation

To evaluate the pullout behavior of the corroded straight steel fibers in UHPC, a full dog-bone shaped specimen was fabricated and tested. Its geometry is shown in Fig. 1; it had a cross-sectional area of $25 \times 25\ mm^2$, and a length of 75 mm. A single steel fiber was affixed to a very thin polyethylene film at the center of the mold. To pull the fiber out only from one side (intentionally), two different embedment lengths of 10 and 20 mm were applied at both sides of the mold in Fig. 1.

Because the fibers in the composites are randomly oriented and dispersed, most fibers are inclined in the direction of the tensile force, and only few fibers are aligned [32]. It is well known that the pullout behavior of the straight steel fibers in

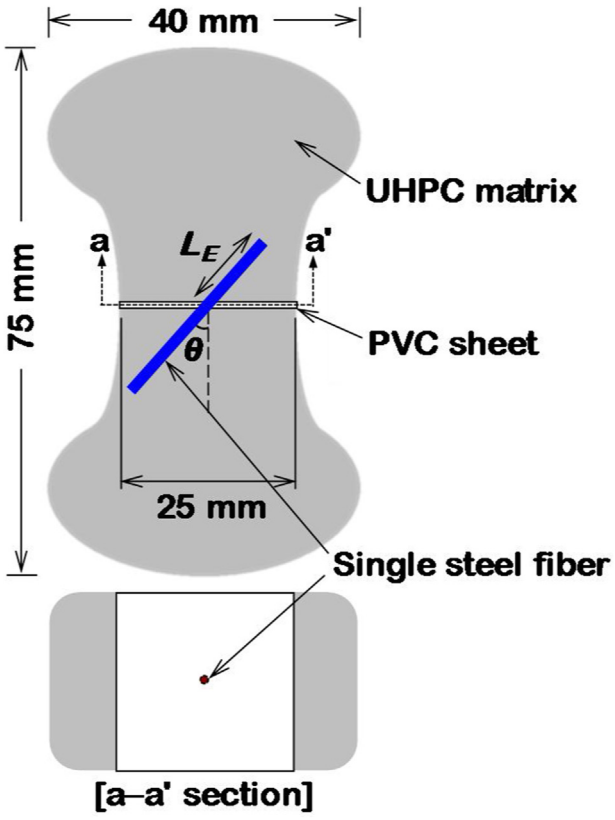

Fig. 1 – Schematic description of geometrical details of dog-bond specimen.

UHPC is affected by its inclination angle [33]; therefore, two different angles, i.e., 0° (aligned) and 45° (inclined) were considered. To assign the inclination angle accurately, a protractor was used, and one side of the fiber, (the longer one) was affixed in a proper position using a form board. Another side, having a shorter embedment length of 10 mm, which is a potential pullout side, was first cast in the mold and cured in a laboratory room at ambient temperature of about 20 °C for 48 h. Then, the mold was removed and the other side was cast in the mold and cured for further 48 h at the same room condition. After that, the specimens were demolded and immersed in a water tank with a temperature of 90° for 48 h, in accordance with a Federal Highway Administration (FHWA) recommendation [34], to promote the strength development of the UHPC matrix.

2.5. Fiber pullout test setup

To evaluate the pullout behavior of artificially corroded fibers in UHPC, a static pullout test machine was utilized, as shown in Fig. 2. The dog-bone shaped specimen was inserted into a steel grip jig, and a pullout force was monotonically applied at a constant loading rate of 0.018 mm/s. At least five specimens were used for each variable to obtain an average value. The rate was controlled by a speed of crosshead, and the applied force was measured using a 3-kN capacity load cell connected to the machine. By assuming that the elastic deformation of the specimen and the jig are negligibly small, the fiber slip was directly measured from the stroke movement. The static

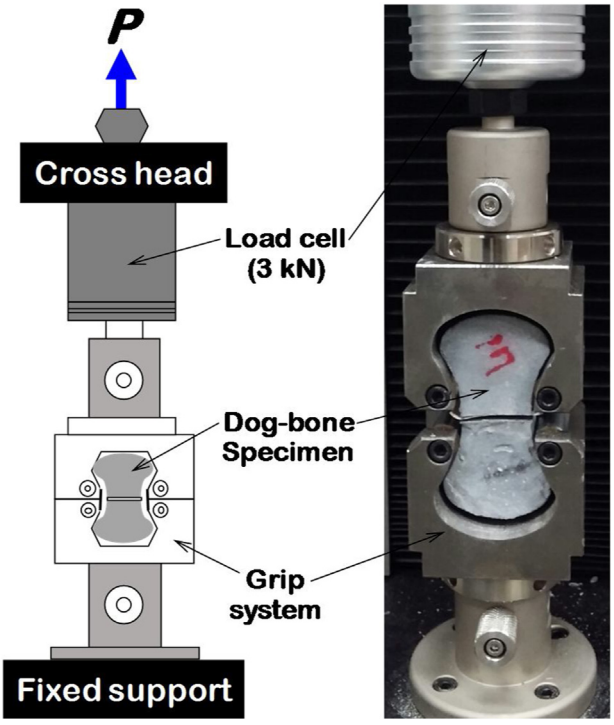

Fig. 2 – Fiber pullout test setup.

pullout load and displacement were measured by means of a data acquisition system using a TDS-540.

3. Results and discussion

3.1. *Microstructural investigation*

3.1.1. *Surface roughness*

To investigate the effect of the corrosion degree and cleaning process on the surface condition of straight steel fibers, SEM images on their surface were obtained, and are summarized in Fig. 3. The plain fibers exhibited a fairly smooth surface, whereas the unwashed, corroded fibers were obviously covered with rust caused by iron oxidation. Because the rust forms irregularly and the images only cover a very small area, the amount of rust detected by the SEM images had no correlation with the overall degree of corrosion. However, the surface roughness of the unwashed, corroded fibers generally increased with the corrosion degree increasing. For instance, more severe grooves formed on the surface of the fiber nearby the location in which rust formed when the degree of corrosion was high. This was more evident in the images of the washed, corroded fiber samples in Fig. 3. Because these fibers were cleaned using the method explained above, most of the surface rust was eliminated; therefore, the surface damaged by steel corrosion was exposed. It was obvious that more severe and abundant grooves formed on the surface of the washed fiber samples with the corrosion degree increasing. Thus, it can be concluded that the surface roughness of the steel fibers generally increases with the corrosion degree increasing for both the unwashed and washed samples.

The three-dimensional (3D) AFM images of the surface of the fibers with various degrees of corrosion are also shown in Fig. 4. Since some of highly corroded fibers, e.g., C10U, C15U, and C15W, exceeded the maximum capacity of AFM machine that is 10 μm in Z-axis (height) direction, their AFM images couldn't be obtained. The plain straight steel fiber had a smooth curvilinear surface, and thus, it was well fitted by a second-degree polynomial function. To evaluate the surface roughness precisely, excluding the effect of the fiber curvature, the shape of the plain fiber was first fitted by a second-degree polynomial equation with a high coefficient of determination (R^2 = 0.99), and the heights of all corroded fibers were subtracted from the fitted curve to obtain the pure surface roughness. The calibrated images of the surface roughness of plain and corroded fibers are thus summarized in Fig. 4. It is obvious that the smooth surface of steel fiber became rougher owing to the corrosion process and increased degree of corrosion in Fig. 4a. After the pulling out process, the direction of furrows was consistently parallel to the longitudinal direction of fiber (Fig. 4b), because some of surface rust was peeled off for the unwashed case and the stiff particles at the fiber-matrix interface scratched its surface.

The surface roughness was obviously increased by fiber corrosion, caused by a process of oxidation and formation of iron oxide. Interestingly, the surface roughness was found to increase with the degree of corrosion increasing, and the washed fibers had a higher roughness than the unwashed fibers with the same corrosion degree. In order to quantify this observation, the surface roughness was evaluated by means of the following equation.

$$Ra = \frac{1}{n}\sum_{i=1}^{n}\left|y_i\right| \quad (1)$$

where y_i is the height of the i^{th} point (nm). Using the height of the pixel coordinate, a surface roughness parameter, *Ra*, was extracted from the images. This parameter defines the arithmetical mean value of the height profiles in each sample.

The surface roughness parameters, *Ra*, are also summarized in Fig. 5. Compared to the value obtained for the plain fiber (*Ra* = 27.1 nm), much higher values were obtained for the corroded fibers regardless if they had been cleaned or not. For instance, the roughness parameter of the C02W fiber was 45.3 nm, which is approximately 1.7 times higher than that of the plain fiber. In addition, highest values of *Ra* were observed for the unwashed corroded fibers at a certain degree of corrosion as compared to those observed for the washed ones in general, owing to the existence of a film of iron oxide (rust layer). The oxidation process occurs irregularly on the fiber surface, and causes an uneven and rough rust layer. The observation that the corroded steel fibers have a rougher surface was also reported by Frazão et al. [18]. However, because the rust layer covering the unwashed fibers was cleaned during the preparation of the washed fibers for the experiment, the initially rough surface became smoother, thus a lower *Ra* value was obtained. For instance, the *Ra* value of C05U was found to be 185.8 nm, which is approximately 159% higher than that (116.9 nm) of C05W fiber. The degree of surface roughness increased with increasing the immersion duration into the

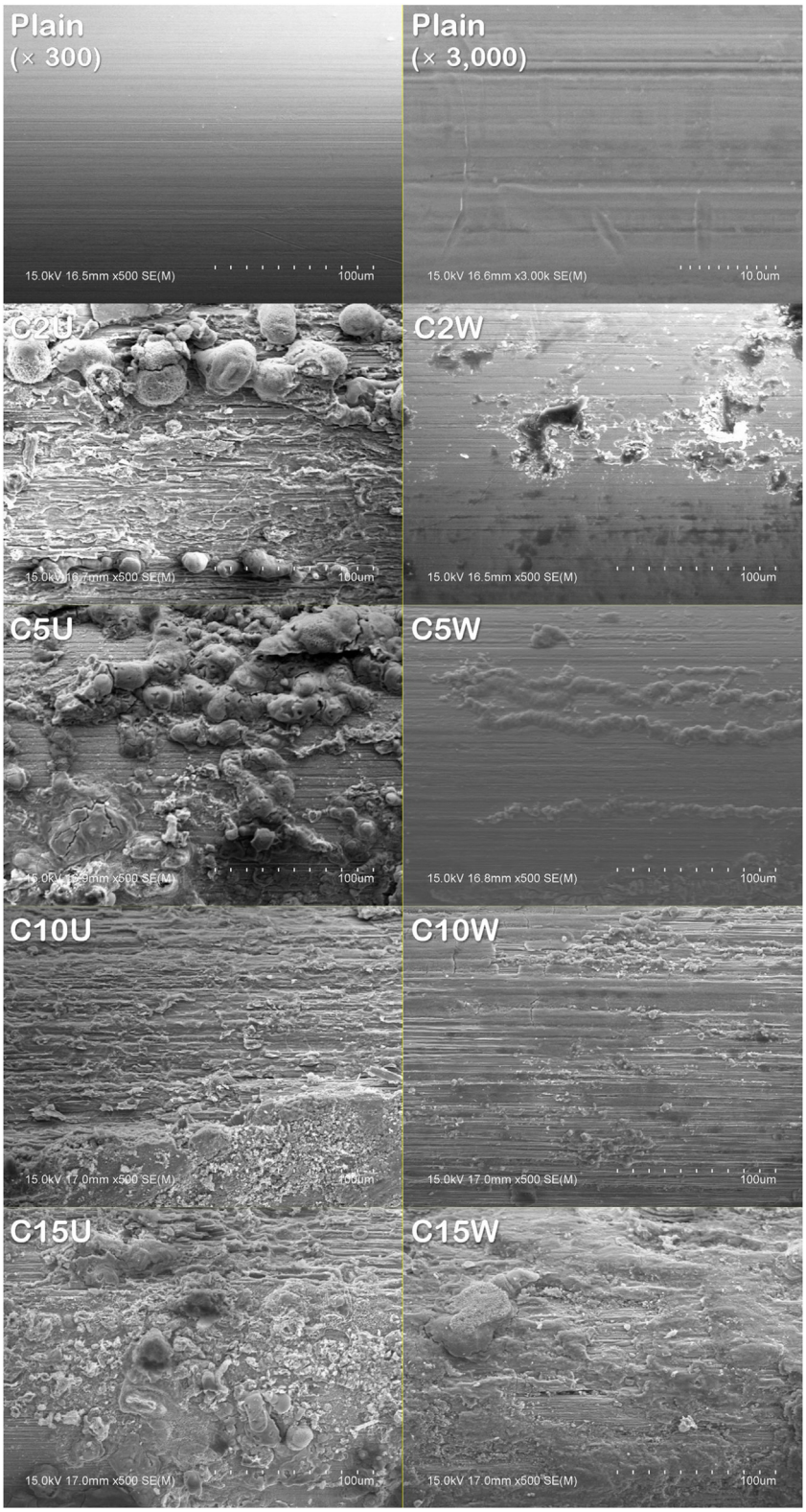

Fig. 3 – SEM images on surfaces of plain and corroded steel fibers

3.5% NaCl solution in general, which is consistent with the findings of Frazão et al. [35] reporting a greater progress of corrosion phenomenon with the immersion time. The variation of surface roughness of plain and corroded fibers before and after the fibers being pulled out from the matrix is investigated in Fig. 5. Because of a high lateral confining pressure due to matrix shrinkage and the presence of rigid hydrate particles at the interface, a number of grooves parallel to the longi-

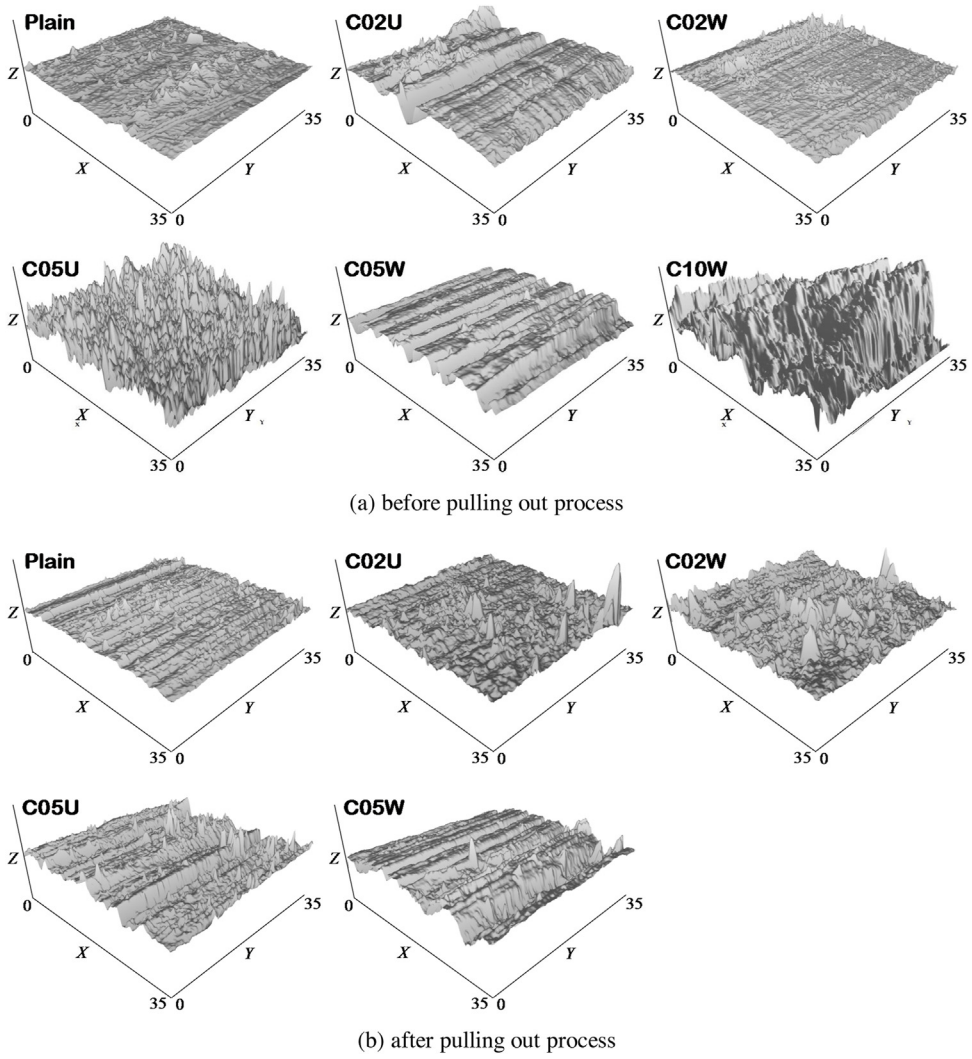

Fig. 4 – AFM images on fiber surface for roughness evaluation: (a) before and (b) after pulling out process.

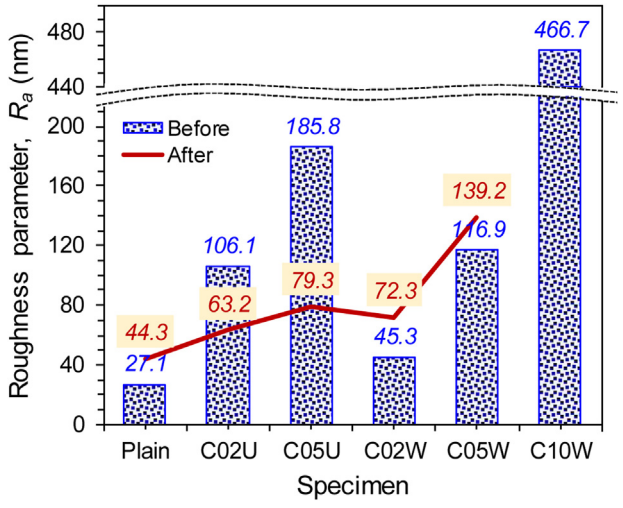

Fig. 5 – Summary of surface roughness parameter (R_a).

tudinal direction of fiber formed in the plain specimen after the completion of the pullout process (Fig. 4b). This is consistent with the findings of Wille and Naaman [36] and Yoo et al. [37], who reported evident surface scratches on straight steel fibers after being pulled out from the UHPC matrix. The abraded fiber surface in Fig. 4b indicates that a portion of it had been peeled off and stacked in the interface between the fiber and matrix, which helped to sustain a high pullout load until a large-magnitude slip occurred. Because of this mechanism, the surface roughness of the plain fiber increased during the pulling out process. The surface roughness of washed, corroded fibers increased in a similar way, which was mainly due to the rigid interfacial hydrate particle forming surface scratches in the direction parallel to the pullout force while trying to contrast the pullout. The post-pullout AFM images of the washed, corroded fibers were thus quite similar to those of the plain fibers. On the contrary, the surface roughness of the unwashed, corroded fibers decreased due to the pulling out process since the fiber surface, rugged by a film of iron oxide, was peeled off during the pullout, producing a relatively smoother fiber surface characterized by a lower roughness

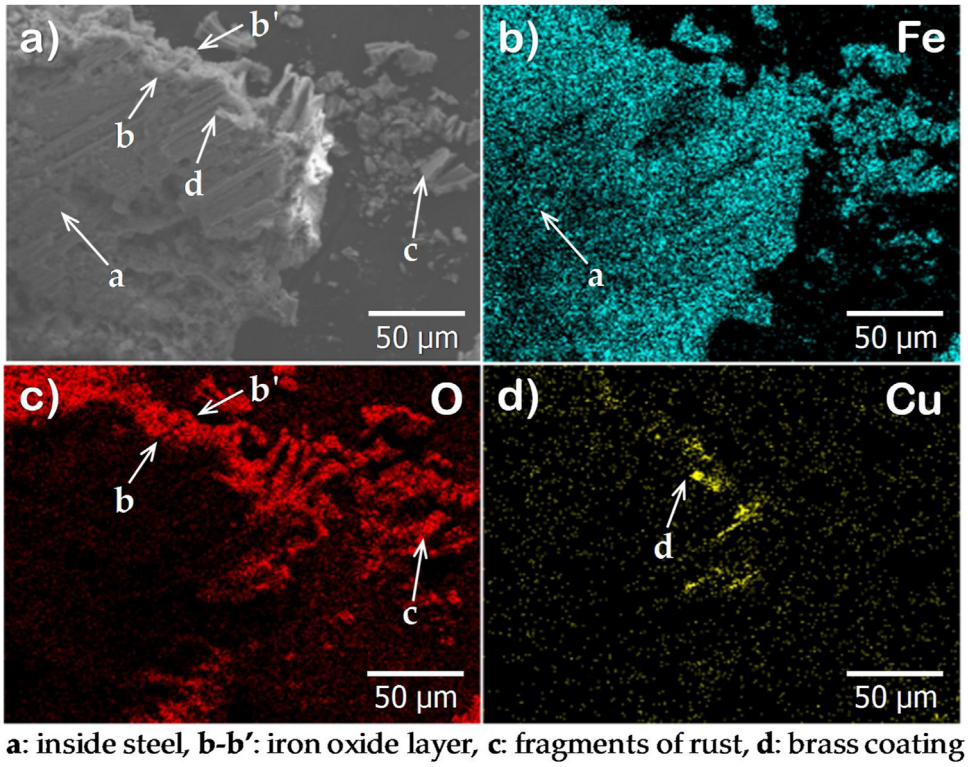

Fig. 6 – Corrosion of steel fiber: (a) SEM image and (b–d) element mapping images of Fe, O, and Cu components.

parameter (*Ra*). Although there existed a film of iron oxide, the surface of the unwashed, corroded fiber was moderately scratched in the direction parallel to the pullout load, in a similar way to what occurred to the plain and washed fibers. The corroded fibers lost a higher amount of steel, which was abraded away from their surface, compared to that lost by the plain fibers; the abraded steel remained stacked at the fiber-matrix interface, and may have been responsible of the stronger pullout resistance exhibited by these samples.

3.1.2. *A film of iron oxide*

To verify the corrosion of the steel fibers and the formation of a film of iron oxide on their surface, an SEM image was taken on the rust layer detached from a steel fiber (C05U), as shown in Fig. 6a. The high-strength steel fibers used for making the UHPFRC are generally brass-coated [38]. Brass is mostly composed of copper (Cu). An EDX mapping analysis was thus conducted. The analysis pointed out that iron (Fe) and oxygen (O) were predominant around the detached particle (Fig. 6b and c). In addition, because the steel fiber is brass-coated, an EDX mapping image for copper (Cu) was also taken along with those for Fe and O (Fig. 6d). Because the rust layer had detached from the steel fiber, a great proportion of steel was detected (i.e., the iron (Fe) component), whereas the periphery of the particle was constituted by a layer of iron oxide, which is indicated by the symbol O in the figure. Only a very little amount of copper (Cu) was detected, and originated from the periphery of the detached fragment of rust. Based on the SEM and EDX mapping analyses (Fig. 6), it could be thus verified that a film of iron oxide formed on the surface of the steel fiber after a continued exposure to the NaCl solution. This occurs because of the corrosion process, which possibly influences the pullout performance of the steel fiber.

3.2. *Pullout load versus slip response*

Fig. 7 summarizes the average pullout load and slip curves for non-corroded and corroded steel fibers in UHPC. Regardless of the presence of corrosion and its degree, the pullout load steeply increased initially with a minor increase of the slip. Then, after reaching the peak point, it gradually decreased until the slip reached approximately 10 mm, which was the initial embedment length. In the portion of the test during which the load was increasing, the fiber was chemically bonded, and then partially de-bonded from the matrix due to a nonlinear bond stress distribution along the length. The pullout load increased rapidly because the tip of the fiber remained at its initial location. Immediately after the maximum load was reached, the fiber became fully de-bonded, and began to be pulled out from the matrix steadily. Mainly due to the reduced embedded length, the pullout load decreased. Because the interface between the fiber and the UHPC matrix is tightly filled with hydrates, de-bonded particles, and filaments abraded away from the surface of the steel fiber, neither a sudden drop of the pullout load just after reaching its maximum point (observed in ordinary concrete by different static and kinetic frictions), nor a concave post-peak pullout load-slip response were obtained. Owing to a slight end deformation caused by the manufacturing process, the pullout load rapidly dropped near the fiber end, as shown in Fig. 7a. This is consistent with findings of previous studies [38,39].

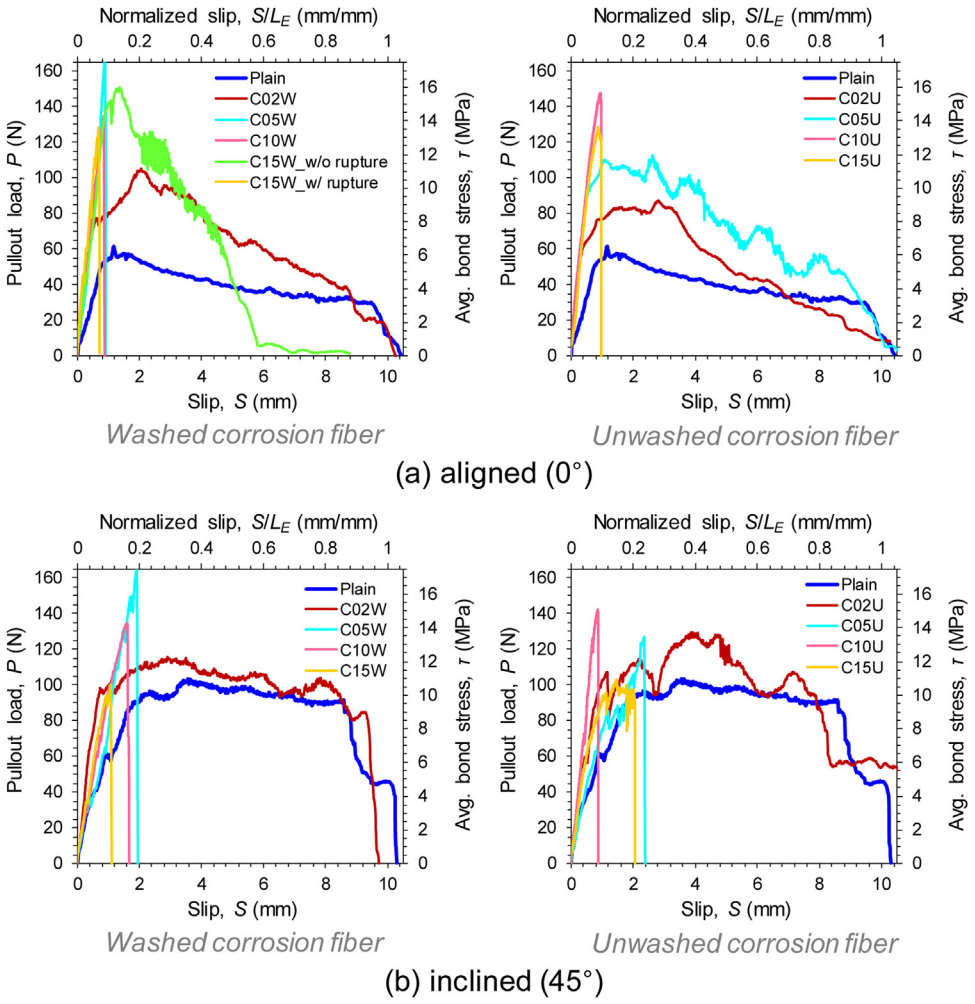

Fig. 7 – Pullout load-slip curves of plain and corroded fibers at (a) aligned (0°) and (b) inclined (45°) conditions.

It was evident that the maximum pullout load of the straight steel fibers in UHPC is enhanced by surface corrosion (Fig. 7), which is consistent with the findings of Frazão et al. [18], mainly due to the increased surface roughness. Moreover, beyond a certain corrosion degree, the failure mode changed from pullout to rupture. For instance, a sudden drop of the pullout load immediately after reaching the maximum point was observed for the steel fibers with a degree of corrosion of 10%, due to their premature breakage. This is caused by the enhanced interfacial frictional resistance caused by the roughened fiber resulting from corrosion and weakening of the fiber section. As can be seen in Fig. 5, the surface roughness of the steel fibers increased with the corrosion degree increasing, resulting in a higher pullout resistance. Chun et al. [40] have also reported, very recently, that the pullout resistance of straight steel fibers in UHPC can be significantly improved by making scratches on the surface of the fibers using sandpaper. Some of these fibers even exhibit a slip-hardening response, which has been barely observed for straight steel fibers.

The enhanced pullout resistance of the corroded steel fibers was attributed to a mechanical anchoring produced by the roughened surface, and the abrasion of more steel fibers, which accumulate at the interface and increase the frictional shear resistance. This explanation can be verified by comparing the surface roughness of plain and corroded steel fibers in UHPC before and after the pullout tests in Figs. 4 and 5. The plain steel fiber had quite a smooth surface before the test, whereas the surface of the pulled-out fiber was noticeably scratched in longitudinal direction due to the fact that hydrated particles at the interface suppressed the pullout, consistent with the findings of Chun et al. [40]. On the other hand, the surface of the unwashed, corroded steel fibers was rougher before the test, but became smoother after the test because a portion of uneven fiber surface was chafed by the interfacial frictional resistance, and stacked in the interface. So, a higher pullout load was maintained until large slip for the corroded fiber specimen compared to that of the plain fibers in Fig. 7a. Fig. 8 shows the SEM-EDX mapping images of the C02U fiber after the completion of the pullout test for quantifying Fe, O, and Cu that remained on the fiber's surface. Because the iron oxide film being eliminated during the pulling out process, mostly Fe was detected from the fiber surface, whereas the contents of O and Cu were relatively minor. Based on the EDX analysis in Fig. 9, even though there are several impurities, detected from particles of cement matrix, the apparent concentrations of Fe, O, and Cu were found to

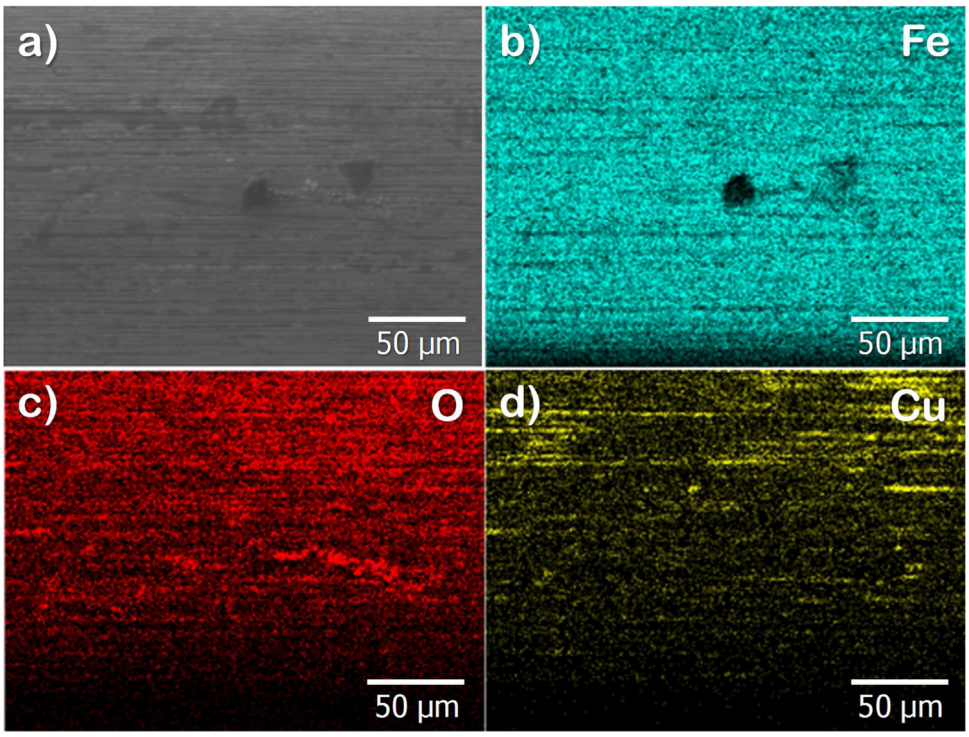

Fig. 8 – Surface characteristics of C02U fiber after a complete pullout: (a) SEM image and (b–d) element mapping images of Fe, O, and Cu components.

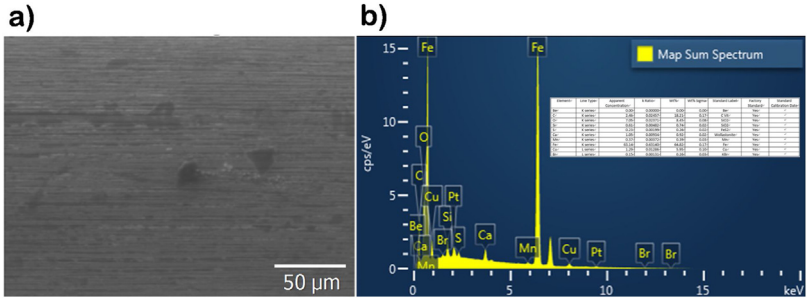

Fig. 9 – EDX analytical results of C02U fiber after a complete pullout: (a) SEM image and (b) EDX results.

be approximately 63.1, 7.1, and 1.3, respectively. The slope of the softening part of the load-slip curve was higher for the corroded fiber specimens compared to that exhibited by the plain specimens because the former provided a higher maximum pullout load at the identical embedment length of 10 mm. The corroded fiber specimens also exhibited more variability in the softening curves, relative to that of plain specimens. This might be due to the stick-slip phenomenon, which occurs if the frictional coefficient is very large and variable, hindering a steady and continuous increase of slip.

By cleaning the rust layer from the corroded surface of the fibers, a higher pullout resistance was generally obtained, as shown in Fig. 7a, yet there was no effect of the surface cleaning on the shape of the pullout load versus slip curve. Because the rust layer on the corroded steel fibers deteriorates the adhesion to the cement matrix substantially, the unwashed, corroded fibers provided lower maximum pullout loads than the washed ones. In particular, at the corrosion degree of 5%, the washed, corroded fibers were ruptured prematurely, and yielded much higher maximum pullout load than the unwashed ones, which showed a complete pullout failure mode. Beyond the 5% corrosion degree, most of the washed, corroded fibers exhibited a rupture failure mode, while the unwashed, corroded fibers started to rupture at a corrosion degree of 10%. Although they showed the rupture failure mode consistently, the maximum pullout load generally decreased with the corrosion degree increasing, which was caused by the decreased cross-sectional area of the fiber. Thus, the fibers with a higher corrosion degree were ruptured at a lower pullout load level. Interestingly, one half of the C15W fibers was ruptured, whereas the remaining fibers were completely pulled out from the matrix, as shown in Fig. 7a. However, although some of the C15W fibers were completely pulled out from the matrix without any breakage (which was confirmed by the fact that the length of the pulled-out fiber was identical to the initial embedment length of 10 mm), the pullout load decreased to almost zero after a shorter slip distance (approximately 6 mm). To verify this unusual obser-

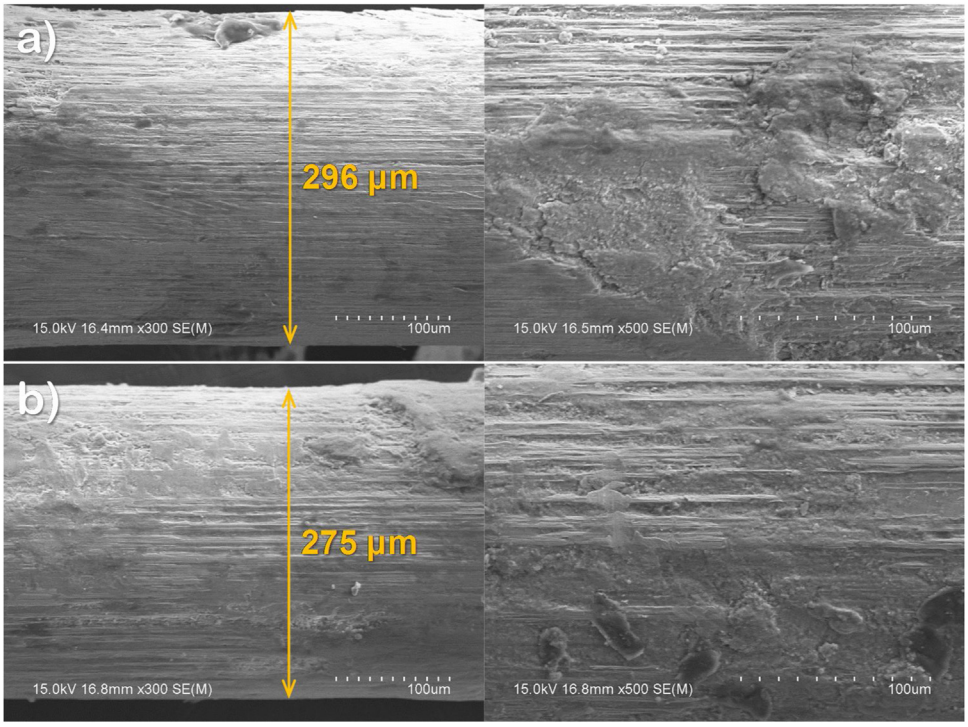

Fig. 10 – SEM images on surface of C15W fiber according to the location: (a) at the exit and (b) at the end of fiber.

vation, SEM images of the surface of the pulled-out C15W fiber at various locations were obtained (Fig. 10) and analyzed. The diameter of the fiber varied according to the location owing to the non-uniform degree of corrosion: an evidently smaller diameter was detected near the end of the fiber compared to that near the exit. This indicates that the partial C15W fibers were easily and rapidly pulled out from the matrix beyond a certain slip without any significant resistance at the interface because of their reduced diameter. Thus, it can be rationally inferred that a portion of the C15W fibers ruptured because they had the smallest diameter at the embedded zone between the exit and end of the fiber. In summary, the failure mode of highly corroded fibers changed according to the location of at which they had the smallest diameter; moreover, if the minimum diameter is found near the fiber end, the fibers can be completely pulled out from the matrix without breakage even at high corrosion degrees.

The pullout behaviors of inclined plain and corroded steel fibers in UHPC are shown in Fig. 7b. Compared to the aligned fiber specimens, they exhibited lower initial pullout stiffness due to a progressive formation of matrix spalling, which is consistent with the findings of a previous study [41]. Due to the lower stiffness of the inclined fiber specimens, their slip capacities were also obviously higher than those of the aligned fiber specimens. It is known that, for the fibers, the resistance to pullout from the cement matrix is influenced by the inclination angle because of the snubbing and matrix spalling effects [42], and a significant matrix spalling in straight steel fibers in UHPC is only obtained if the fibers are inclined [43]. The plain fiber and the washed and unwashed, corroded fibers with a degree of corrosion of 2%, i.e., specimens C02W and C02U were pulled out from the UHPC matrix without any breakage. Furthermore, they maintained the external pullout load well, after reaching the initial peak point, up to a quite large slip value of approximately 8 mm (Fig. 7b). This was attributed to an additional frictional resistance generated at the fiber exit by a resistance, R, acting in orthogonal direction with respect to the longitudinal direction of the fiber (i.e., snubbing effect). Once the corrosion degree exceeds 5%, the washed and unwashed, corroded fibers were all ruptured because the force R caused stress concentration locally, leading to the easier rupture of the fibers at smaller stress levels. Therefore, these corroded fibers exhibited an abrupt drop of the pullout load immediately after reaching the peak load. Although there is a wide variation in the initial pullout stiffness, the corroded fiber specimens generally provided higher stiffness compared to the plain specimens, which were similar to those exhibited by the aligned fibers.

3.3. *Average bond strength*

The mathematical equations for the pullout parameters are summarized in Appendix. The effect of the corrosion degree on the average bond strength is illustrated in Fig. 11. The average bond strength of plain straight steel fibers in UHPC was found to be approximately 6.9 MPa, which is consistent with the range of previously reported values, 5.2–9.0 MPa [38,40,44]. The average bond strength increased with the steel fiber corrosion with respect to the case without corrosion. For the washed specimens, it increased with the degree of corrosion increasing up to 5%, as shown in Fig. 11a. At higher degrees of corrosion, the average bond strength was slightly reduced. The washed, corroded fibers were completely pulled out from the matrix when their corrosion degree was lower than 5%.

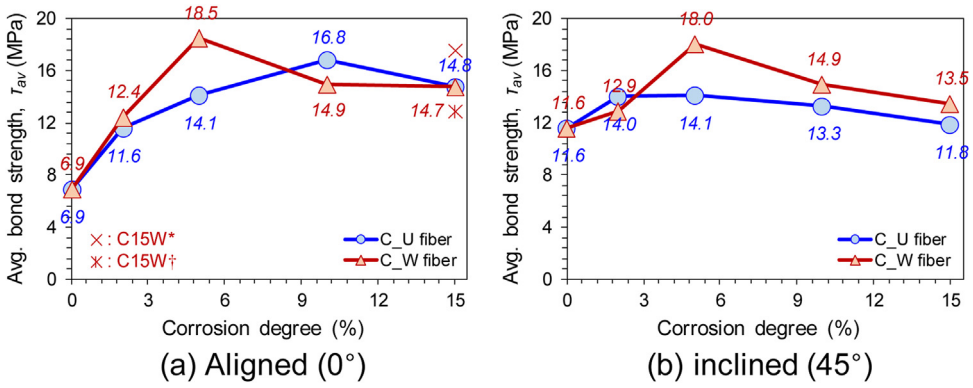

Fig. 11 – Effect of corrosion degree on the average bond strength: (a) aligned (0°) and (b) inclined (45°) conditions [Note: C_U fiber = unwashed corrosion fiber series, C_W fiber = washed corrosion fiber series, * = pulled out, and † = ruptured].

Thus, the interfacial bond strength could be improved by the surface corrosion due to the increased roughness in Fig. 5. However, from the 5% corrosion level, the fibers started to be ruptured due to excessive bond strength and exhibited a slight decrease of bond strength. Thus, it can be concluded that the increase of interfacial bond strength by surface corrosion on the straight steel fibers in UHPC is limited because of the premature breakage of the fibers by weakened fiber section. Similarly, the unwashed, corroded fibers provided higher average bond strengths than the plain fibers, and the effectiveness increased with the corrosion degree increasing up to a certain point (10%; see Fig. 11a). Because the increase rate of bond strength was lower for the unwashed fibers, it reached the maximum value at a higher degree of corrosion. After that, owing to the same reasons pointed out for the washed specimens, the average bond strength was rather decreased by the rupture. Owing to the rust layer between the core of the fiber and the cement matrix, the unwashed fibers generally provided smaller bond strengths than the washed ones at an identical corrosion degree. The highest average bond strength was found to be approximately 18.5 MPa for the corroded steel fibers in UHPC, which is even higher than that (12.5 MPa) of the half-hooked steel fibers, and slightly lower than that (19.9 MPa) of the twisted steel fibers in the same matrix [41]. This strength is also approximately 3 times higher than that exhibited by the plain fibers.

When the fibers were inclined by 45° with respect to the direction of the pullout force, higher bond strengths were recorded for both the plain and the corroded steel fibers in UHPC; this was mainly caused by an additional frictional resistance at the exit by the snubbing effect [42]. Similar observations have been reported by Lee et al. [33] and Yoo and Kim [41]: the highest bond strength for straight steel fibers in UHPC was found for inclination angles between 30° and 45°. The most significant increase in bond strength was observed in the plain fiber specimen, approximately 68% (from 6.9 to 11.6 MPa), and the beneficial effect of inclining the fibers decreased with the corrosion degree increasing up to 5%. For instance, the average bond strength of the inclined unwashed fiber (i.e., C5U) in UHPC was identical to that of the aligned one (14.1 MPa). For corrosion degrees higher than 5%, even higher average bond strengths for the aligned corroded fibers in UHPC were observed compared to those of the inclined fibers (Fig. 11). This is due to the fact that both the aligned and inclined corroded fibers with degrees of corrosion of 5% were all ruptured. In particular, the inclined fibers were ruptured at lower stress levels with respect to the aligned ones owing to the local stress concentration by the orthogonal force R. The washed and unwashed, corroded fibers in UHPC exhibited an increase of average bond strength for corrosion degrees up to 5% in specimens in which they were inclined; on the other hand, the bond strength decreased for corrosion degrees higher than 5%.

3.4. *Pullout energy and equivalent bond strength*

Fig. 12 summarizes the pullout energy and equivalent bond strength of plain and corroded fibers in UHPC. Similar to the average bond strength, the pullout energy and the equivalent bond strength of plain fibers were enhanced by surface corrosion with the corrosion degree increasing up to 2% and 5%, respectively, for the washed and unwashed specimens at the aligned condition. The pullout energy of the plain fiber in UHPC was found to be 389.6 N·mm ($\times 10^{-3}$ J), and its equivalent bond strength (8.3 MPa) was higher than the average bond strength (6.9 MPa). Because the equivalent bond strength was calculated based on the pullout energy, the two quantities exhibited a similar dependence to the corrosion degree (Fig. 12a). The pullout energy increased with the corrosion degree increasing up to the certain points; beyond those point, it substantially decreased due to a change in failure mode from pullout to fiber rupture. The washed, corroded fibers yielded higher interfacial pullout resistances compared to the unwashed ones. Therefore, they exhibited a significant deterioration of pullout energy (or equivalent bond strength) earlier than the unwashed fibers, at smaller degrees of corrosion. The pullout energy of steel fibers in UHPC seemed not affected by the corrosion degree if the fibers were ruptured. For aligned fibers, the highest pullout energy (715.8 N·mm) was found for the unwashed fiber specimen with 5% corrosion degree, which is approximately 2 times higher than that observed for the plain fiber specimen. This difference is attributed to the enhanced frictional shear resistance at the interface in the former.

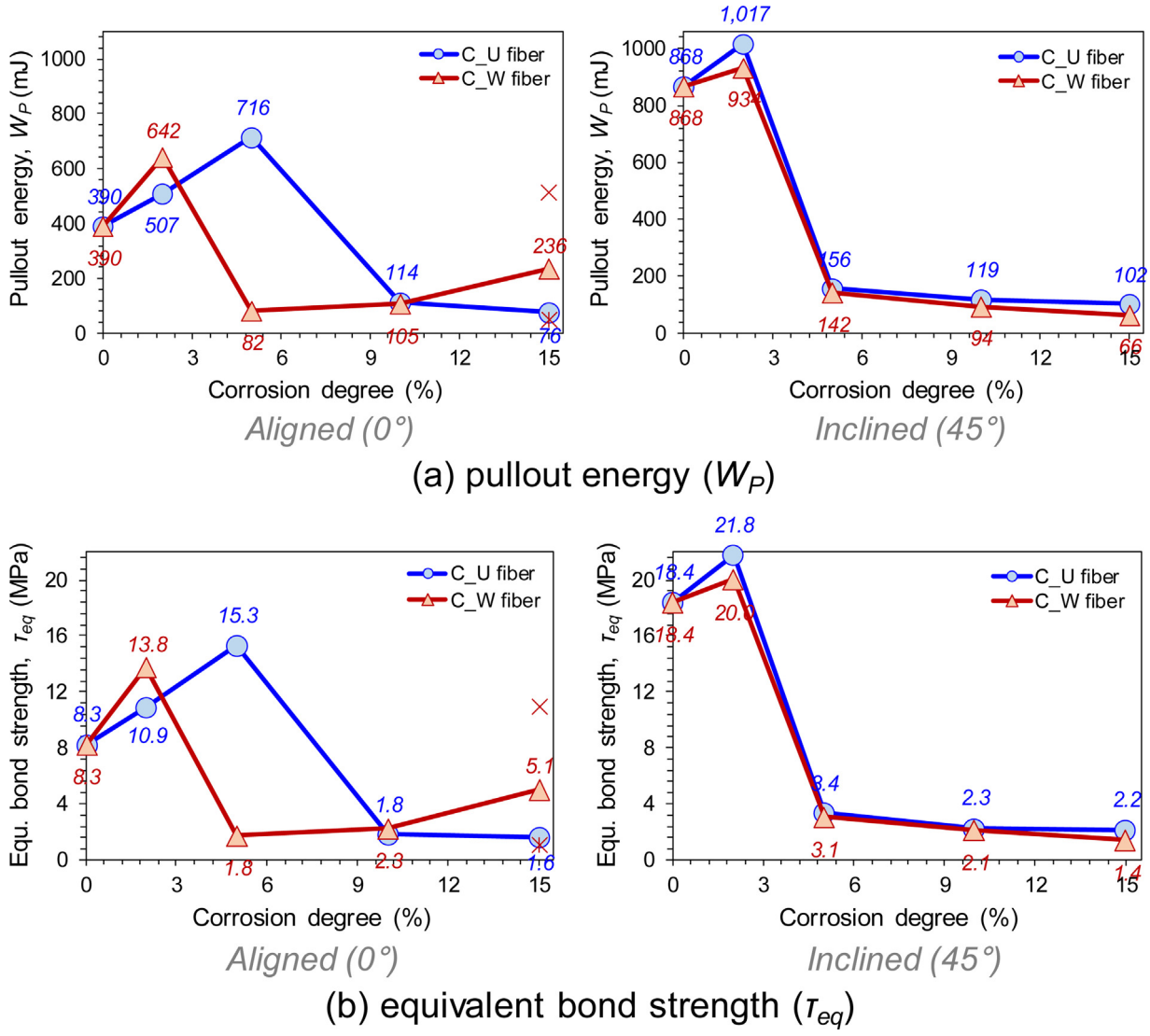

Fig. 12 – Effect of corrosion degree on the (a) pullout energy (W_P) and (b) equivalent bond strength (τ_{eq}) [Note: C_U fiber = unwashed corrosion fiber series, C_W fiber = washed corrosion fiber series, * = pulled out, and † = ruptured].

Higher pullout energy and equivalent bond strength were found in the inclined fiber specimens that failed according to the pullout failure mode (up to a corrosion degree of 2%; see Fig. 12b) with respect to those exhibited by the aligned specimens. This is attributed to the higher pullout resistance, which is maintained for longer time, up to larger slip values. However, for degrees of corrosion above 2%, the inclined, corroded fibers exhibited a substantial decrease of the pullout energy and equivalent bond strength due to the failure mode that exhibited premature rupture. The effectiveness of surface corrosion of the inclined straight steel fibers in UHPC in enhancing the pullout energy absorption capacity was observed if the fiber was completely pulled out from the matrix, without any breakage. Owing to the enhanced interfacial shear resistance and reduced cross-sectional area of the corroded steel fibers, however, they ruptured when the corrosion degree was 2% or higher if the fibers were inclined. This resulted in a poorer energy absorption capacity. In summary, it can be concluded that the surface corrosion of straight steel fibers in UHPC is effective in improving the pullout energy absorption capacity only if the fibers are completely pulled out (without rupture occurring) regardless of their inclination angle. Therefore, the corrosion degree of the straight steel fibers in UHPC structures needs to be limited below the value of 2% to achieve excellent fiber bridging capability and ductility without incurring in fiber breakage.

3.5. *Maximum fiber tensile stress*

As shown in Fig. 13, the maximum tensile stress in the fibers also increased with the degree of surface corrosion increasing prior to the occurrence of fiber rupture, in accordance with the increase of maximum pullout load. The maximum fiber tensile stress became greater at higher corrosion degrees because of the enhanced interfacial frictional resistance. For example, at a corrosion degree of 15%, the maximum fiber tensile stress was found to be 2,135 MPa on average, which is approximately 2.3 times higher than that of the plain fibers

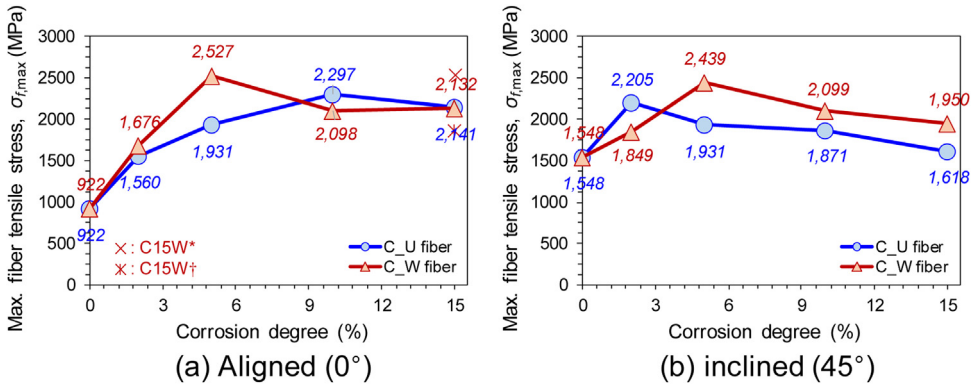

Fig. 13 – Effect of corrosion degree on the maximum fiber tensile stress at (a) aligned (0°) and (b) inclined (45°) conditions [Note: C_U fiber = unwashed corrosion fiber series, C_W fiber = washed corrosion fiber series, * = pulled out, and † = ruptured].

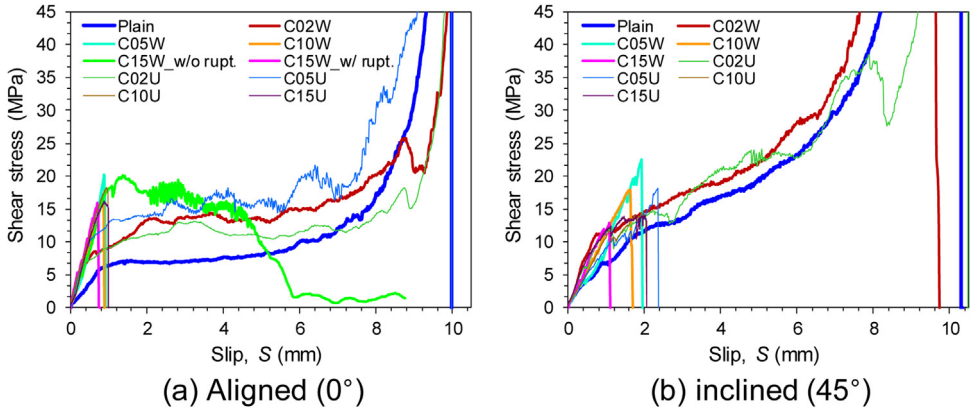

Fig. 14 – Shear stress-slip curves: (a) aligned (0°) and (b) inclined (45°) conditions.

in Fig. 13a. However, this is only approximately 85% of the ultimate tensile strength of the steel fiber as provided by the manufacturer, which might be attributed to a variable the corrosion degree according to the location on the fiber. Even though we immersed the steel fibers in NaCl solutions in the same way to obtain an uniform corrosion along the fibers, the actual degree of corrosion on the fiber surfaces was different according to the location on the fiber, resulting in a slightly lower tensile strength compared to the value given by manufacturer. A similar trend was also observed for the inclined fiber specimens in Fig. 13b. The maximum fiber tensile stresses of the inclined fibers were generally slightly smaller than those of the aligned ones at higher corrosion degrees, mainly caused by the additional resisting force at the exit acting orthogonally to the direction of the fiber length and generating a local stress concentration on it. The maximum tensile stress of inclined, corroded steel fibers in UHPC was generally decreased with the corrosion degree increasing as they were ruptured. Marković [45] reported that the increase in the cross-sectional area of the steel fibers is responsible for the higher bending stiffness. The higher degree of surface corrosion decreased the cross-sectional of the fiber and the bending stiffness, which might be one of the reasons for the decrease of maximum fiber tensile stress for the inclined, corroded fibers with the corrosion degree increasing (Fig. 13b).

3.6. *Shear stress and slip response*

Fig. 14 shows the relationship between the shear stress and the slip for plain and corroded steel fibers in UHPC. The shape of the curve for the plain straight steel fiber was quite similar to those reported by previous studies [38,39]. The steep increase of shear stress at the slip levels approaching the value of the embedded length (10 mm), is caused by its end deformation resulting from a fiber cutting process [38]. The interfacial shear stress of approximately 7 MPa was maintained well up to a slip value of approximately 5–6 mm, which is half of the embedment length, without exhibiting any obvious increase in the case of plain fiber, indicating a slip-softening behavior (Fig. 14a). For specially fabricated fibers, e.g., twisted and sanded steel fibers, which showed a slip-hardening behavior, it has been observed in a previous study [40] that the interfacial shear stress continuously increased from the initial stage of slip. However, this phenomenon was not observed in this study. The corroded steel fibers (washed and unwashed) all exhibited higher shear stress values at corresponding slip levels compared to that exhibited by the plain fiber. Higher degrees of corrosion generally resulted in higher shear stress levels, as shown in Fig. 14a. For instance, a shear stress of approximately 10 MPa was maintained in the C02U specimen, and a higher shear stress (approximately 14 MPa) was observed in the C05U specimen with a higher corrosion degree

when the fibers were aligned. The increased interfacial shear stress is caused by the roughened surface of the fiber produced by the corrosion, and by the higher amount of fiber filaments abraded and accumulated at the interface. In addition, the washed, corroded fibers exhibited a higher shear stress compared to that exhibited by the unwashed fibers at corresponding corrosion degrees because the rust layer had an adverse effect on the interfacial bond with the cement matrix. Although the surface corrosion effectively increased the interfacial shear strength of the plain steel fiber in UHPC, it still produces a slip-softening pullout response when the fiber is aligned. It is interesting to notice that the shear stress of the corroded fibers increased more sharply at the initial stage of loading and was higher than that exhibited by the plain fiber in Fig. 14a. This might be caused by the actual bonding area between the fiber and the matrix which increased because of the uneven surface and thanks to the bearing force acting on bulgy parts and potholes on the fiber surface, thus requiring an increased pullout force to detach the fiber from the matrix. Some corroded specimens with high corrosion degree exhibited a sharp drop of shear stress immediately after reaching the peak stress caused by the fiber rupture. This indicates that the enhancement of frictional shear resistance by surface corrosion is limited by the fiber rupture; therefore, if the ultimate tensile strength of the fiber increases, a better pullout resistance in terms of higher bond strength and pullout energy can be achieved thanks to a high corrosion degree. The pulled out C15W fibers exhibited a unique shape of the shear stress-slip curve. They provided the highest shear stresses at smaller slip values (below approximately 2 mm), which was attributed to the increased surface roughness. However, for higher values of slip, a gradual decrease of shear stress with the slip increasing was observed, which is in contrast to the behavior of the other samples, due to their reduced diameter toward the fiber end.

As shown in Fig. 14b, a significantly higher and monotonically increasing shear stress was observed for both plain and corroded steel fibers in UHPC in an inclined condition, with respect to that exhibited by the same fibers installed in an aligned condition. In particular, the improvement of the interfacial shear resistance of the plain fiber caused by the inclination was more significant than the improvement observed on the corroded fibers. Owing to the excellent enhancement, the inclined plain fiber in UHPC even exhibited a pullout load-slip curve analogous to the slip-hardening behavior shown in Fig. 7, exhibiting a higher pullout load carrying capacity which was maintained beyond the full debonding point. The surface corrosion also led to an enhanced interfacial shear resistance of the inclined fiber in UHPC, which was similar to that observed in the aligned case. In Fig. 14b, it can be seen higher shear stresses at the initial stage of loading were observed in the corroded specimens (i.e., C02W and C02U); however, the slopes of their shear stress-slip curves were quite similar to that exhibited by the plain specimen. This indicates that the beneficial effect surface corrosion on the interfacial shear resistance of straight steel fibers in UHPC is more pronounced for aligned fibers than for the inclined ones. The beneficial effect of the surface roughness of the steel fiber on its interfacial shear resistance might be damped by the complex snubbing and matrix spalling effects when the fiber is inclined. For corrosion degrees higher than 2%, the inclined, corroded fibers were all ruptured, and thus exhibited a sudden drop of stress immediately after reaching the peak point. Even though the corroded fiber specimens provided higher initial shear stiffness compared to the plain specimen, the degree of stiffness increase was small, and the data deviation was higher compared to that observed for the aligned fibers. The rate of shear stress increase versus slip became higher at slip values higher than approximately 6 mm, which was attributed to the fiber end deformation, and was analogous to what observed for the aligned fiber specimens (Fig. 14).

4. Conclusions

This study examined the effects of different degrees of surface corrosion of straight steel fibers on the pullout behavior of UHPC. A single-fiber pullout test was conducted with two inclination angles of 0° and 45° to consider the effect of the random fiber orientation in composites. For the case of the corroded fibers, both washed and unwashed samples were prepared to analyze the effects of the rust layer. The SEM and AFM images were also taken for surface roughness evaluation and iron oxide mapping. From the test results and discussion above, the following conclusions are drawn.

1 The surface corrosion of straight steel fibers in UHPC was effective in enhancing the pullout resistance for both aligned and inclined fibers if they are completely pulled out from the matrix without breakage.
2 Surface corrosion on aligned steel fibers was more effective in improving the pullout resistance of UHPC than that on inclined fibers.
3 The higher corrosion degree on the steel fibers resulted in a better pullout resistance up to a certain degree of corrosion, i.e., 2 or 5%, depending on the inclination angle and the washing of the corroded surface. Beyond that, most of the corroded steel fibers were ruptured, resulting in much poorer pullout energy and equivalent bond strength.
4 A 2% corrosion degree was determined as the threshold value for achieving excellent fiber bridging capability in UHPC composites with random fiber orientation.
5 The washed, aligned corroded fibers gave higher bond strengths and pullout energy than the unwashed ones at the same degree of corrosion. The beneficial effect of corrosion vanished when the fibers were inclined and prematurely ruptured.
6 A higher interfacial shear resistance was observed in the corroded and inclined fibers from the UHPC matrix as compared to that exhibited by plain and aligned fibers. Most of the aligned steel fibers in UHPC exhibited a slip-softening behavior, whereas some of the inclined fibers showed a vague slip-hardening behavior.

Conflict of interest

There is no conflict of interest.

Acknowledgements

This work was supported by the National Research Foundation of Korea (NRF) grant funded by the Korea government (MSIT) (No. 2017R1C1B2007589).

Appendix

To evaluate the effect of the corrosion degree on the pullout behavior of straight steel fibers in UHPC quantitatively, several important parameters, i.e., the average and equivalent bond strengths, pullout energy, and maximum fiber tensile stress, were calculated on the basis of the equations described in the following paragraphs.

The average bond strength can be calculated based on the measured maximum pullout load and the initial bonding area between fiber and matrix, which, in turn, is obtained from the known value of the initial embedment length (10 mm), as follows.

$$\tau_{av} = \frac{P_{max}}{\pi d_e L_E} \tag{A1}$$

Here, τ_{av} is the average bond strength (MPa), P_{max} is the maximum pullout load (N), d_e is the effective fiber diameter (mm) considering the degree of fiber corrosion, and L_E is the initial embedded length of the fiber (mm). Because Eq. (1) relies on the maximum load, the maximum resistance to pullout can be evaluated.

For achieving an excellent toughness or energy absorption capacity of the composites, the fibers need to be pulled out steadily with a high level of energy absorption. This desirable quality can be evaluated by calculating the fiber pullout energy, which is related to the area subjected to the pullout load and the slip curve, and it is given by Eq. (A2) as follows.

$$W_P = \int_{s=0}^{s=L_E} P(s)\, ds \tag{A2}$$

Here, W_p is the fiber pullout energy (N·mm), s is the slip (mm), and $P(s)$ is the slip-dependent pullout load (N).

If it is assumed that the interfacial bond strength between the fiber and the matrix remains constant throughout the entire bonding length, an equivalent bond strength can be calculated from the pullout energy, W_P. Given a triangular-shaped load-slip curve and equally distributed frictional shear stress through the entire bonding length, the equivalent bond strength can be calculated by the following equation.

$$\tau_{eq} = \frac{2W_p}{\pi d_e L_E^2} \tag{A3}$$

Here, τ_{eq} is the equivalent bond strength (MPa).

The steady-state flat crack formation, required for obtaining a strain-hardening behavior with formation of multiple microcrack, is only achieved if the bridging capacity of the fiber is very high. If the fibers are ruptured before reaching the complete pullout, the crack width will increase rapidly, failing to achieve the strain-hardening characteristics. To assess this behavior, the maximum fiber tensile stress based on the maximum pullout load and cross-sectional area of the fiber is calculated from Eq. (4), and compared with its ultimate tensile strength.

$$\sigma_{f,max} = \frac{P_{max}}{A_e} \tag{A4}$$

Here, $\sigma_{f,max}$ is the maximum tensile stress in the fiber (MPa), and A_e is the effective cross-sectional area of the fiber considering the degree of fiber corrosion (mm^2), given by $\pi {d_e}^2/4$.

REFERENCES

[1] Richard P, Cheyrezy M. Composition of reactive powder concretes. Cem Concr Res 1995;25(7):1501–11.
[2] ACI Committee 239. Ultra-high performance concrete. Toronto, Ontario, Canada: ACI Fall Convention; 2012.
[3] AFGC. Ultra high performance fibre-reinforced concretes. Bagneux, France: Interim Recommendations, AFGC publication; 2013.
[4] Voort TLV. Design and field testing of tapered H-shaped ultra high performance concrete piles. Iowa, USA: MS Thesis, Iowa State University; 2008. p. 229.
[5] Shaheen E, Shrive NG. Optimization of mechanical properties and durability of reactive powder concrete. ACI Mater J 2006;103(6):444–547.
[6] Blunt J, Jen G, Ostertag CP. Enhancing corrosion resistance of reinforced concrete structures with hybrid fiber reinforced concrete. Corros Sci 2015;92:182–91.
[7] Hou J, Chung DDL. Effect of admixtures in concrete on the corrosion resistance of steel reinforced concrete. Corros Sci 2000;42(9):1489–507.
[8] Mihashi H, Ahmed SFU, Kobayakawa A. Corrosion of reinforcing steel in fiber reinforced cementitious composites. J Adv Concr Tech 2011;9(2):159–67.
[9] Jen G, Ostertag CP. Experimental observations of self-consolidated hybrid fiber reinforced concrete (SC-HyFRC) on corrosion damage reduction. Constr Build Mater 2016;105:262–8.
[10] Berrocal CG, Löfgren I, Lundgren K, Tang L. Corrosion initiation in cracked fibre reinforced concrete: influence of crack width, fibre type and loading conditions. Corros Sci 2015;98:128–39.
[11] Sahmaran M, Li VC, Andrade C. Corrosion resistance performance of steel-reinforced engineered cementitious composite beams. ACI Mater J 2008;105(3):243–50.
[12] Shaikh FUA, Mihashi H, Kobayakawa A. Corrosion durability of reinforcing steel in cracked high-performance fiber-reinforced cementitious composite beams. J Mater Civil Eng 2014;27(8):04014228.
[13] fib Bulletin No. 34: Model Code for Service Life Design, International Federation for Structural Concrete (fib), Lausanne, Switzerland, 2006, pp. 116.
[14] Fantilli AP, Cavallo AD, Pistone G. Fiber-reinforced lightweight concrete slabs for the maintenance of the Soleri Viaduct. Eng Struct 2015;99:184–91.
[15] Lee SJ, Yoo DY, Moon DY. Effects of hooked-end steel fiber geometry and volume fraction on the flexural behavior of concrete pedestrian decks. Appl Sci (Basel) 2019;9(6):1241.
[16] Chiaia B, Fantilli AP, Vallini P. Evaluation of minimum reinforcement ratio in FRC members and application to tunnel linings. Mater Struct 2007;40(6):593–604.

[17] Yoo DY, Yoon YS. A review on structural behavior, design, and application of ultra-high-performance fiber-reinforced concrete. Int J Concr Struct Mater 2016;10(2):125–42.
[18] Frazão C, Barros J, Camões A, Alves AC, Rocha L. Corrosion effects on pullout behavior of hooked steel fibers in self-compacting concrete. Cem Concr Res 2016;79:112–22.
[19] Kosa K, Naaman AE. Corrosion of steel fiber reinforced concrete. ACI Mater J 1990;87(1):27–37.
[20] Granju JL, Balouch SU. Corrosion of steel fibre reinforced concrete from the cracks. Cem Concr Res 2005;35(3): 572–7.
[21] Banthia N, Foy C. Marine curing of steel fiber composites. J Mater Civil Eng 1989;1(2):86–96.
[22] Hashimoto K, Toyoda T, Yokota H, Kono T, Kawaguchi T. Tension-softening behavior and chloride ion diffusivity of cracked ultra-high strength fiber reinforced concrete. In: RILEM-*fib*-AFGC international symposium on ultra high performance fibre-reinforced concrete, Marseille, France; 2014. p. 257–64.
[23] Beglarigale A, Yazıcı H. Electrochemical corrosion monitoring of steel fiber embedded in cement based composites. Cem Concr Compos 2017;83:427–46.
[24] Balouch SU, Forth JP, Granju JL. Surface corrosion of steel fibre reinforced concrete. Cem Concr Res 2010;40(3):410–4.
[25] Pyo S, Tafesse M, Kim H, Kim HK. Effect of chloride content on mechanical properties of ultra high performance concrete. Cem Concr Compos 2017;84:175–87.
[26] Abbas S, Soliman AM, Nehdi ML. Exploring mechanical and durability properties of ultra-high performance concrete incorporating various steel fiber lengths and dosages. Constr Build Mater 2015;75:429–41.
[27] Yoo DY, Min KH, Lee JH, Yoon YS. Shrinkage and cracking of restrained ultra-high-performance fiber-reinforced concrete slabs at early age. Constr Build Mater 2014;73:357–65.
[28] Yoo DY, Kim S, Kim MJ. Comparative shrinkage behavior of ultra-high-performance fiber-reinforced concrete under ambient and heat curing conditions. Constr Build Mater 2018;162:406–19.
[29] Yoo DY, Kim MJ. High energy absorbent ultra-high-performance concrete with hybrid steel and polyethylene fibers. Constr Build Mater 2019;209:354–63.
[30] Graybeal BA. Flexural behavior of an ultrahigh-performance concrete I-girder. J Bridge Eng 2008;13(6):602–10.
[31] ASTM C1437. Standard test method for flow of hydraulic cement mortar. West Conshohocken, PA: ASTM International; 2013. p. 1–2.
[32] Yoo DY, Kang ST, Yoon YS. Effect of fiber length and placement method on flexural behavior, tension-softening curve, and fiber distribution characteristics of UHPFRC. Constr Build Mater 2014;64:67–81.
[33] Lee Y, Kang ST, Kim JK. Pullout behavior of inclined steel fiber in an ultra-high strength cementitious matrix. Constr Build Mater 2010;24(10):2030–41.
[34] Graybeal BA. Material property characterization of ultra-high performance concrete (No. FHWA-HRT-06-103); 2006.
[35] Frazão C, Díaz B, Barros J, Bogas JA, Toptan F. An experimental study on the corrosion susceptibility of Recycled Steel Fiber reinforced Concrete. Cem Concr Compos 2019;96:138–53.
[36] Wille K, Naaman AE. Pullout behavior of high-strength steel fibers embedded in ultra-high-performance concrete. ACI Mater J 2012;109(4):479–87.
[37] Yoo DY, Choi HJ, Kim S. Bond–slip response of novel half-hooked steel fibers in ultra-high-performance concrete. Constr Build Mater 2019;224:743–61.
[38] Wille K, Naaman AE. Effect of ultra-high-performance concrete on pullout behavior of high-strength brass-coated straight steel fibers. ACI Mater J 2013;110(4):451–61.
[39] Yoo DY, Park JJ, Kim SW. Fiber pullout behavior of HPFRCC: effects of matrix strength and fiber type. Compos Struct 2017;174:263–76.
[40] Chun B, Yoo DY, Banthia N. Achieving slip-hardening behavior of sanded straight steel fibers in ultra-high-performance concrete. Cem Concr Compos 2020, under review.
[41] Yoo DY, Kim S. Comparative pullout behavior of half-hooked and commercial steel fibers embedded in UHPC under static and impact loads. Cem Concr Compos 2019;97:89–106.
[42] Li VC, Wang Y, Backer S. Effect of inclining angle, bundling and surface treatment on synthetic fibre pull-out from a cement matrix. Compos 1990;21(2):132–40.
[43] Yoo DY, Chun B, Kim JJ. Effect of calcium sulfoaluminate-based expansive agent on rate dependent pullout behavior of straight steel fiber embedded in UHPC. Cem Concr Res 2019;122:196–211.
[44] Tai YS, El-Tawil S, Chung TH. Performance of deformed steel fibers embedded in ultra-high performance concrete subjected to various pullout rates. Cem Concr Res 2016;89:1–13.
[45] Marković I, Ph.D. Thesis High-performance hybrid-fibre concrete: development and utilisation. Technische Universität Delft; 2006.